Simulation of the Solution Structure of the H-*ras* p21–GTP Complex†

C. K. Foley,‡ L. G. Pedersen,‡,§ P. S. Charifson,∥ T. A. Darden,*,‡ A. Wittinghofer,⊥ E. F. Pai,⊥ and M. W. Anderson*,‡

Laboratory of Molecular Toxicology, National Institute of Environmental Health Sciences, Research Triangle Park, North Carolina 27709, Department of Chemistry, University of North Carolina, Chapel Hill, North Carolina 27599-3290, Cray Research, Inc., P.O. Box 12746, Research Triangle Park, North Carolina 27709, and Abteilung Biophysik, Max-Planck-Institut für Medizinische Forschung, Jahnstrasse 29, 6900 Heidelberg, FRG

Received November 20, 1991; Revised Manuscript Received March 24, 1992

ABSTRACT: An unconstrained simulation of the GTP-bound form of the H-*ras* protein p21 is performed in an aqueous environment with charge-neutralizing counterions. The simulation is compared to the 1.35-Å structure of Pai et al. [(1990) *EMBO J. 9*, 2351] and a proposed alternate structure, in which the loop at residues 60–65 is modeled into a form which may activate a water molecule for the GTP hydrolysis. The simulation suggests that some protein intermolecular H-bond contacts which are present in the crystal structure are lost in the solvation process and this loss may lead to localized refolding of the molecule. For instance, we find that the γ-phosphate of the GTP has somewhat weaker contact with the protein in the simulation structure. The antiparallel β-sheet (residues 38–57) partially melts. The 60–65 loop, which is hypervariable in the X-ray study, is initially relatively distant from the γ-phosphate region. However, this loop moves so as to sample the space around the γ-phosphate. For a significant fraction of the simulation time, forms similar to the alternate structure are observed, and a water molecule is localized near the hydrolytic site. The molecular dynamics simulations of p21–GTP in solution support a postulated hydrolysis mechanism for the biological inactivation of the nucleotide complex based on crystallographic data.

The *ras* family of protooncogenes are of particular interest since they have been implicated in the development of numerous tumors. H-*ras*,[1] K-*ras*, and N-*ras* can acquire transforming activity by a point mutation in their coding sequence. The reports of X-ray crystal structure determinations of the G-nucleotide bound forms of the normal and oncogenic *ras* proteins (Pai et al., 1989; Milburn et al., 1990) give hope that an unraveling of the sequence of events leading to signal transduction and possibly subsequent carcinogenesis via mutant forms of the protein may soon be forthcoming.

The *ras* gene products are 21 000-Da proteins (p21) which bind guanine nucleotides with high affinity and are thought to be involved in various signal transduction pathways in many cell types (McCormick, 1989; Bourne et al., 1991; Valencia et al., 1991). The p21–GDP complex receives a signal from an upstream element (i.e., an activated membrane-bound receptor), and the GDP is exchanged for GTP to convert the inactive p21–GDP complex to the active p21–GTP complex (Downward et al., 1990). The p21–GTP is able to transmit the signal downstream to an appropriate target. The active GTP complex with p21 is converted to the inactive GDP complex by hydrolysis of GTP to GDP. The p21 protein itself possesses intrinsic GTPase activity; however, in vivo, this intrinsic activity is greatly enhanced by GAP (GTPase activating protein). GAP can enhance the GTPase activity of p21 by at least a factor of 4×10^3 (Bollag & McCormick, 1991). After the discovery of GAP, it was shown that the main biochemical difference between oncogenic p21s with mutations in codon 12, 13, or 61 and wild-type p21 is the ability of GAP to induce GTP hydrolysis in the active p21–GTP complex. The GAP-induced hydrolysis can be as much as 1000 times faster in the wild-type p21 than in these mutant forms of *ras* (Gibbs et al., 1988; Vogel et al., 1988). These mutant forms thus remain in the active GTP form much longer than the wild-type, and presumably the continual transmission of a signal by the mutant forms is responsible, at least in part, for the oncogenic properties. Mutation studies have identified the sequence 30–40 as the region of GAP binding (Adari et al., 1988); this region has also been shown to have substantial motion relative to the remainder of the molecule in crystalline nucleotide bound forms (Milburn et al., 1990). To study the motion of this region as well as that of other functional domains, the molecular dynamics (MD) method was employed.

Molecular dynamics is a technique that permits the limited simulation of macromolecules in solution (McCammon & Harvey, 1987). It is an open question as to how much structural change might generally be expected when a protein is taken from its crystal environment and placed in solution; it is perhaps reasonable to anticipate significant changes in parts of the structure that are involved in protein–protein contacts in the crystal. Differences between crystal structures and 2D NMR solution structures of proteins are known (Bax, 1989; Baldwin et al., 1991). If the changes are significant so as to involve major reorganization of the protein, then it is unlikely that several hundred picoseconds of simulation will be sufficient to describe the "solution" refolding process.

† This work was supported in part by Grant HL27995 from the National Heart, Lung, and Blood Institute.

* Author to whom correspondence should be addressed.
‡ National Institute of Environmental Health Sciences.
§ University of North Carolina.
∥ Cray Research, Inc.
⊥ Max-Planck-Institut für Medizinische Forshung.

[1] Abbreviations: amu, atomic mass units; BPTI, bovine pancreatic trypsin inhibitor; c-*ras*^{H}, cellular H-*ras*; DSSP, *d*efine *s*econdary *s*tructure of *p*roteins computer program; GAP, GTPase activating protein; GDP, guanosine diphosphate; GppNp, guanyl-5′-yl imidodiphosphate; GTPγS, guanosine 5′-*O*-(3-thiotriphosphate); GTP, guanosine triphosphate; GTPase, guanosine-5′-triphosphatase; H-*ras*, Harvey ras; MD, molecular dynamics; p21–GTP, 1:1 complex of p21 and GTP; v-*ras*^{H}, viral H-*ras* p21 (G12R, A59T).

0006-2960/92/0431-4951$03.00/0

Simulation by molecular dynamics, however, hopefully has an important role to play in the description of the early refolding events that take place upon solvation.

In the simulation described here, we have taken considerable care to equilibrate an environment of water and counterions in which to simulate the motion of p21–GTP as it moves from its crystal form to its solution form. The p21–GTP system has no stabilizing disulfide bonds and is highly ionic at physiological pH. Both factors might be expected to destabilize the molecular system in aqueous solution. Consequently, this system constitutes an excellent test of the theoretical methods.

Methods

The AMBER version 3A (Weiner et al., 1984, 1986) molecular dynamics program was supplied by Peter Kollman of UCSF. The simulations utilized the all-atom force field (Weiner et al., 1986) with a single nonbonded cutoff of 9.0 Å for energy minimization and a twin cutoff, which is discussed below, for molecular dynamics. The molecules were immersed in a box of TIP3P water (Jorgensen et al., 1983) (approximately 9500 waters solvated the macromolecule). As such, the results reported here represent one of the largest proteins studied to date [Swope and Andersen (1990) have performed simulations on 10^6 atomic particles] which does not have stabilizing covalent disulfide links. All covalent bonds involving hydrogen were constrained; a mass of 3 amu was used for all hydrogens. The simulations were performed at 300 K (after initial stepwise heating over the first 3 ps of the simulation), the integration step size was 1 fs, and the nonbonded list was updated every 20 steps. When the nonbonded list was updated, the forces were also corrected to include the effect of electrostatic interactions in the range between 9.0 and 22.0 Å. The inclusion of this long-range force correction, which had been suggested by Berendsen et al. (1986), proved to be essential for stabilizing the structure over a long simulation. Several test simulations performed with a 9.0-Å cutoff without the long-range correction developed instabilities within approximately 50 ps; in these simulations the helix structures were stable but many ionic interactions were not. The consequences of various implementations of long-range cutoff have also been studied by Loncharich and Brooks (1989) and by Smith and Pettitt (1991).

Appropriate code modifications were made to ensure that the protein and water bath did not have diverging temperatures. The partial atomic charges of the singly protonated nucleotide GTP were estimated by fitting electrostatic potentials found by ab initio quantum chemical calculations (Frisch et al., 1988; 3-21G* basis set, resulting charges scaled to the 6-31G** level) by a Langrangian multiplier technique (Chirlian & Francl, 1987a,b). The computations were performed on a Cray Y-MP computer at the North Carolina Supercomputing Center (Research Triangle Park, NC) or on a Silicon Graphics Iris 4D/380-VGX workstation. Essential graphics were performed on the Iris using the program MULTI (Darden et al., 1991).

Several modifications were made to AMBER to increase the throughput: (a) The SHAKE algorithm was modified to conform to the modified Newton's method suggested by Ryckaert et al. (1977). This algorithm replaces the normal AMBER iterative SHAKE procedure by a linearization of the simultaneous quadratic equations. SHAKE is known to be slowly convergent on cyclic structures, such as TIP3P water, whereas the modified Newton's method converges rapidly. A speedup of approximately 20% results. (b) Computation of the nonbonded list was modified by implementation of a grid technique. The size of the grid was determined by one-half of the nonbonded cutoff; interactions greater than two grid units apart are not tested. This innovation resulted in a speedup of approximately 20% for our problem. (c) The manner in which the solvent–any atom interactions are computed was modified by preprocessing the nonbonded list of the solvent–any atom interactions, using to advantage the fact that the hydrogens of the rigid TIP3P water have no van der Waals interactions; this implementation, along with preimaging the waters that have a high probability of being imaged (those within one nonbonded cutoff of the box side), led to a speedup of approximately 40%. Finally, the box was recentered to the center of coordinates of the protein at every step; this led to an improvement in the efficiency of the computation by avoiding minimum imaging conflicts. The net increase in speed of these improvements in the code was nearly a factor of 2. Approximately 1 ps of simulation time per 3 cpu·h was obtained on a single Cray Y-MP processing element. A parallel version of the code which utilized multiple processors was constructed.

As a rough check of our procedures, bovine pancreatic trypsin inhibitor (BPTI) was simulated in a large water box (8.0-Å nonbonded cutoff, no long-range correction). One way to compare differences or similarities between two protein structures is to calculate the least squares superposition (Kabsch, 1976, 1978) of the backbone atoms of the two molecules; the result is conventionally expressed as a root mean square (rms) deviation of the optimal superposition. The rms of the backbone atoms of BPTI (simulation compared to crystal) equilibrated by about 35 ps and remained between 1.35 and 1.6 Å for the remainder of the simulation. The rms values are similar to those reported by Berendsen et al. (1986) and to those of Levitt and Sharon (1988).

The p21 simulations are prepared and conducted according to the following protocol:

(1) All covalent hydrogen bonds were minimized (without explicit solvent) while the protein heavy atoms were kept fixed.

(2) The crystallographic protein and water coordinates (Pai et al., 1990) were placed in a large water box (sides were 13 Å from the nearest protein atom); this system was then used to compute the electrostatic potential from the AMBER point charges on a grid about the protein. Positions for neutralizing sodium counterions were defined to be those positions of maximum negative electrostatic potential. The crystallographic waters and added ions were then minimized, with the protein held fixed, using a distance-dependent dielectric constant.

(3) Resolvation was then accomplished by defining a box of water with each side being at least 13 Å from the nearest protein atom. The water molecules were placed so as to have no water oxygen closer than 2.8 Å or water hydrogen closer than 2.0 Å to a protein atom.

(4) The large box of water wan then minimized at constant volume while the protein atoms were held stationary. Twenty picoseconds of dynamics was then performed on the water only.

(5) The water was then reminimized (with the protein held fixed) followed by a minimization of all atoms. The system was now ready for all-atom dynamics.

Results and Discussion

Solvation of the 1.35-Å Crystallographic Structure. The simulation of the solvated 1.35-Å crystallographic structure of Pai et al. (1990) was performed for 200 ps. We have examined the general features of the early refolding that occurs, the details of the crystal contacts that are broken on solvation, and the time dependence of the interactions between the nucleotide and the protein in the early solution structure.

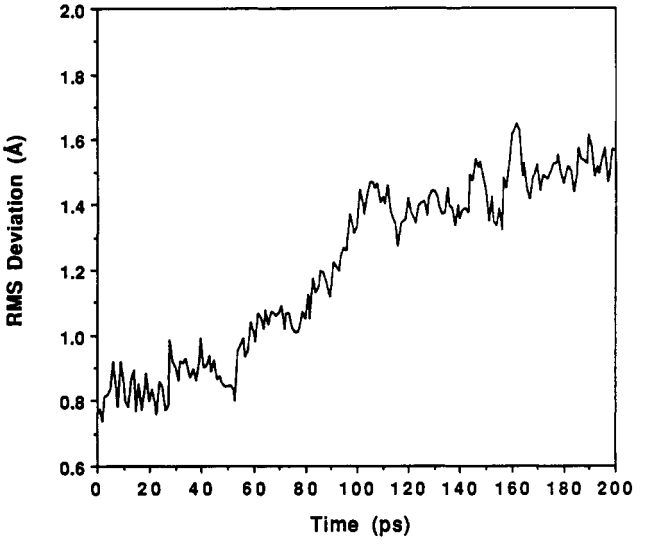

FIGURE 1: rms deviation of the backbone atoms (residues 1–166) of the simulated p21 structure from the X-ray crystal structure (Pai et al., 1990) over the simulation (0–200 ps). The protein has undergone several minimizations at 0 ps; see Methods.

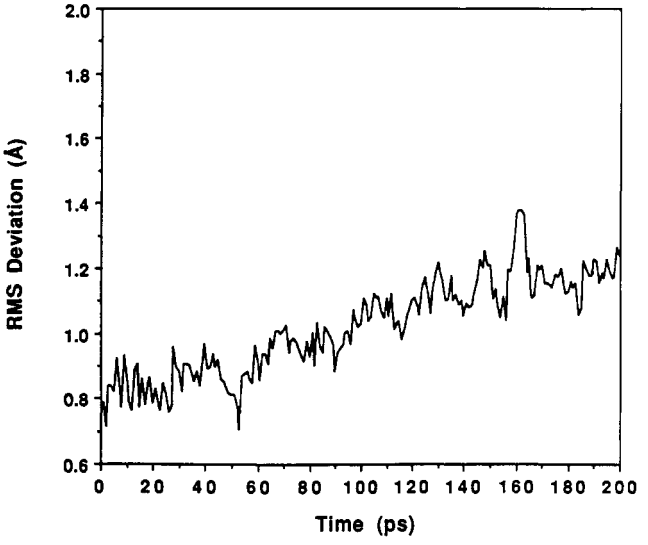

FIGURE 2: rms deviation of the backbone atoms (residues 10–59 and 69–156 only) of the simulated p21 structure from the X-ray structure (Pai et al., 1990) over the simulation (0–200 ps).

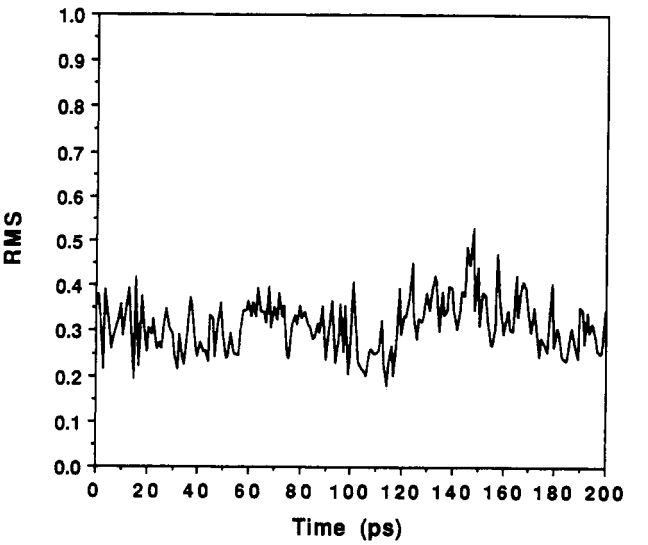

FIGURE 3: rms deviation of the backbone atoms of an extended α-helix (residues 127–138) of the simulated p21 structure from that of the X-ray crystal structure (Pai et al., 1990) over the simulation (0–200 ps).

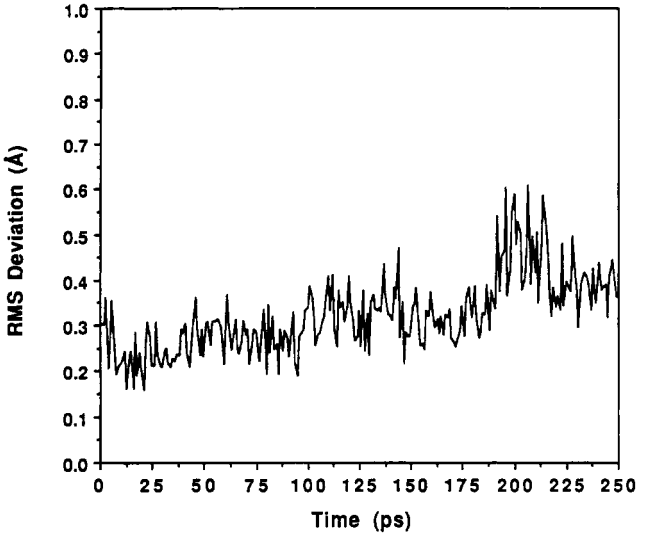

FIGURE 4: rms deviation of the backbone atoms of the pnosphate binding loop (residues 10–18) of the simulated p21 structure from that of the X-ray crystal structure (Pai et al., 1990) over the simulation (0–249 ps).

(*i*) *General Features That Distinguish the Early Solution Structure.* Simulations on bovine pancreatic trypsin inhibitor (BPTI) in solution have shown that the BPTI backbone structure quickly equilibrates in solution (Berendsen et al., 1986); we have verified this with a control simulation on BPTI that we discussed in the Methods section. Equilibration also appears to occur for the p21–GTP simulation although somewhat later ($\sim$160 ps) than for the BPTI case. An rms vs time plot for the backbone atoms is shown in Figure 1; the rms function appears to be approaching $\sim$1.60 Å asymptotically. Since large thermal *B* factors were seen for residues 60–68 in the X-ray structure and since it is reasonable to expect that solvation might affect the protein termini, we chose the backbone atoms of residues 10–59 and 69–156 as a basis for comparison to the crystal structure. A plot of the rms of these backbone atoms compared to X-ray is shown in Figure 2. These atoms appear to become equilibrated by $\sim$100 ps with an asymptotic value of $\sim$1.25 Å. Some regions within these sets show considerably less deviation. For instance, the multiturn helix 127–138 (Figure 3) and the phosphate binding loop 10–18 (Figure 4) are stable with rms to the X-ray crystal structure of less than 0.6 Å for the simulation. For the average structure over the last 26 ps of the simulation (174–200 ps), the backbone atoms of residues 10–18 have an rms compared to the crystal structure of 0.31 Å, and the backbone atoms of residues 127–138 have an rms of 0.21 Å compared to the X-ray. An analysis of the secondary structure was performed using the Kabsch/Sander program DSSP (Kabsch & Sander, 1983). The helix counts in the crystal structure and in the average simulation structure (174–200 ps) are remarkably similar; 57 residues are labeled as helix in the crystallographic structure, whereas 61 are labeled helix in the average (174–200-ps) simulation structure. Fifty-six of the 57 residues labeled as helix in the crystal structure have a secondary structure definition identical to that in the average simulation structure. The average simulation structure has an additional turn (65–67) of helix develop at the N-terminus of the 68–74 helix. A substantial unfolding that occurs early in the simulation is the partial melting of the β-sheet framework of the X-ray structure. For instance, the β-sheet hydrogen bonds of Asp38–Asp57 are both broken by 125 ps in the only anti-

Table I: Hydrogen-Bond Interprotein Contacts in the p21–GTP Crystal[a]

molecule 1	molecule 2	distance (Å)
Met1 O	Asp105 O	2.822
Met1 N	Gln25 O	2.841
Met1 H	Asp105 O	2.374
Met1 H	Gln25 O	2.391
Phe28 N	Asp107 $O_{\delta 1}$	2.96
Phe28 H	Asp107 $O_{\delta 1}$	2.10
Glu31 $O_{\epsilon 2}$	Lys88 N_{ζ}	3.19
Glu31 $O_{\epsilon 2}$	Lys88 $H_{\zeta 1}$	2.20
Tyr32 O_{η}	GTP $O_{\gamma 1}$	2.71
Tyr32 H_{η}	GTP $O_{\gamma 1}$	1.77
Pro34 O	Gln61 $N_{\epsilon 2}$	2.53
Pro34 O	Gln61 $H_{\epsilon 2}$	1.56
Arg41 N_{ϵ}	His166 O	3.025
Arg41 H_{ϵ}	His166 O	2.163
Arg41 $N_{\eta 1}$	His166 O	2.925
Arg41 $H_{\eta 1}$	His166 O	2.017
Lys42 N_{ζ}	Glu76 $O_{\epsilon 1}$	3.074
Lys42 $H_{\zeta 1}$	Glu76 $O_{\epsilon 1}$	2.065
Asp47 $O_{\delta 2}$	Glu143 N	3.213
Asp47 $O_{\delta 2}$	Glu143 H	2.279
Asp105 $O_{\delta 2}$	Arg128 $N_{\eta 1}$	2.888
Asp105 $O_{\delta 2}$	Arg128 $H_{\eta 1}$	1.966
Asp154 $O_{\delta 2}$	Arg161 $N_{\eta 2}$	3.175
Asp154 $O_{\delta 2}$	Arg161 $H_{\eta 2}$	2.229
Asp154 $O_{\delta 1}$	Arg161 $N_{\eta 1}$	3.117
Asp154 $O_{\delta 1}$	Arg161 $H_{\eta 1}$	2.271

[a] Pai et al. (1990).

parallel β-sheet (38–57) of the crystal structure. Previously, Yamasaki et al. (1989) had observed a conformational change apparently involving partial β-sheet melting around Ser39/Leu56 when the c-Ha-*ras* gene product *ras*(1–171) underwent GDP → GTPγS exchange. The 174–200-ps average structure has 33 residues labeled as β-sheet by DSSP (Kabsch & Sander, 1983), whereas the crystal structure had approximately 44 residues as β-sheet. All but one of the differences between X-ray and simulation occurred in the antiparallel β-sheet (38–57). All of the 33 residues identified as involved in β-sheets in the simulation structure are also identified with β-sheets in the crystal structure.

(ii) Protein–Protein Contacts That Are Disrupted upon Solvation. The 1.35-Å crystal unit cell of p21 contains only 35% solvent (Pai et al., 1990). This solvent concentration is at the lower end of that normally observed for protein crystals. Consequently, numerous protein–protein contacts are encountered (Table I). Major intermolecular hydrogen bond contacts occur at residues **1**, **25**, **28**, 31, 32, **34**, **41**, 42, **47**, 61, 76, 88, **105**, 107, 128, **143**, 161, and **166**; those contacts in boldface indicate that backbone atoms are involved, and the remaining contacts are of a side-chain–side-chain nature. Significant contacts occur in the same regions that show considerable variance (Figure 5) over the simulation (0–200 ps): N and C termini, residue groups 29–32, 47–48, 60–68, and 105–109. The so-called effector region (residues 30–40) interacts with the X-ray variable region (residues 61–65) through H-bond contacts between residue 34 of one molecule and residue 61 of another molecule. Likewise, residues 1, 41, 42, 47, 76, and 143 are involved directly or indirectly in the β-sheet structure as well as protein–protein contacts. Thus, given the substantial contact regions that are disrupted upon simulation of solvation, the observed pattern of early refolding is perhaps not surprising.

(iii) GTP–Protein Interactions: What is Lost (or Gained) on Solvation? The number of GTP interactions in the average structure (174–200 ps) are fewer than in the crystal structure (Table II). The Mg^{2+} ion, the central atom in the ternary complex, has the same six ligands in both the simulation and

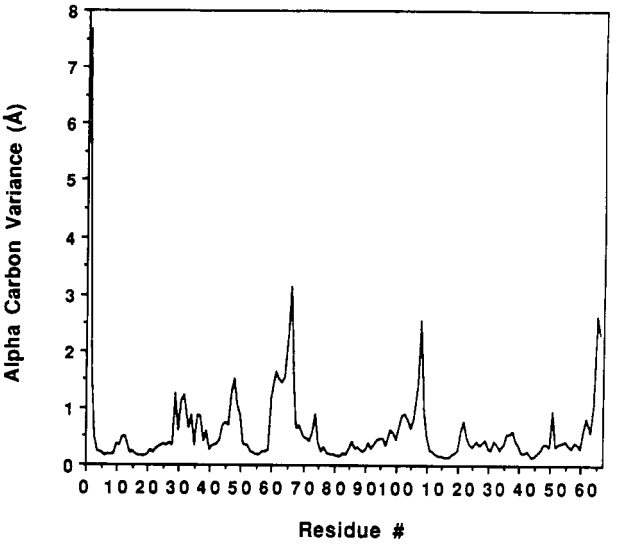

FIGURE 5: Variance ($\langle (x - \langle x \rangle)^2 \rangle$) of the C_α coordinates of p21 during the (0–200-ps) simulation.

Table II: Significant Hydrophilic Interactions of GTP/Mg^{2+} with p21[a]

interactions	X-ray (Pai et al., 1990)	simulation
Mg^{2+}	γ- and β-phosphate, 2 waters, Thr35, Ser17	γ- and β-phosphate, 2 waters,[b] Thr35, Ser17
γ-phosphate	Mg^{2+}, Gly13, Lys16, Thr35, Gly60	Mg^{2+}, Gly60
β-phosphate	Mg^{2+}, Gly13, Gly15, Lys16, Ser17	Mg^{2+}, Gly13, Val14, Gly15, Lys16, Ser17
α-phosphate	Ala18	Gly15
ribose	Val29, Asp30, [Lys117]	Asp30
guanine	Asn116, Asp119, Ala146	Asn116, Asp119, Ser145, Ala146, Lys147

[a] The criterion for a hydrogen-bonded contact is O, N–O, N < 3.5 Å and O, N–H < 2.4 Å. Contacts shown in brackets indicate a near contact, usually the longer criterion met but not the shorter. Ionic contact criterion: <2.5 Å. The simulation structure represents the average structure from 174–200 ps. [b] The water molecules remaining at 200 ps are identical to those of the X-ray crystallographic structure.

crystal structures: an oxygen from each of the β- and γ-phosphates, the side-chain hydroxyls of S17 and T35, and two water molecules. The water molecules bound to the Mg^{2+} ion are the same as those in the X-ray structure; water exchange on the Mg^{2+} did not occur over 200 ps. All details of the magnesium coordination are thus preserved from the crystal structure. The γ-phosphate, however, which has H-bond contacts with G13, K16, T35, and G60 in the crystal structure, retains only the G60 contact in the simulation average structure. The backbone NH interaction of T35 and the side-chain interaction of K16 with the γ-phosphate are weaker in the simulation structure than in the X-ray structure, but it is perhaps significant that they are not completely dissociated. The β-phosphate, on the other hand, has contacts with the amide backbone of residues 13–17. The α-phosphate–Ala18 amide NH contact is replaced by an analogous contact with Gly15. The Val29 contact with the ribose is lost; however, two secure H-bonds remain between the side chains of Asp30 and the hydroxyls of the ribose (O2′ and O3′). The loop contacts of the guanine at N116 and D119 remain. Two strong H-bonds tie residues A146 and K147 to the guanine.

Mutations at G12, with the exception of G12P, are transforming, and so it is of interest to examine motion of this residue. The G12(C_α)–P_γ distance shows considerable variance over the simulation, from 4.9 to 3.7 Å, with an average value of 4.0 Å over the last 26 ps of the simulation. Likewise, the torsion angles defined by the C_α atoms of residues 9–15 change

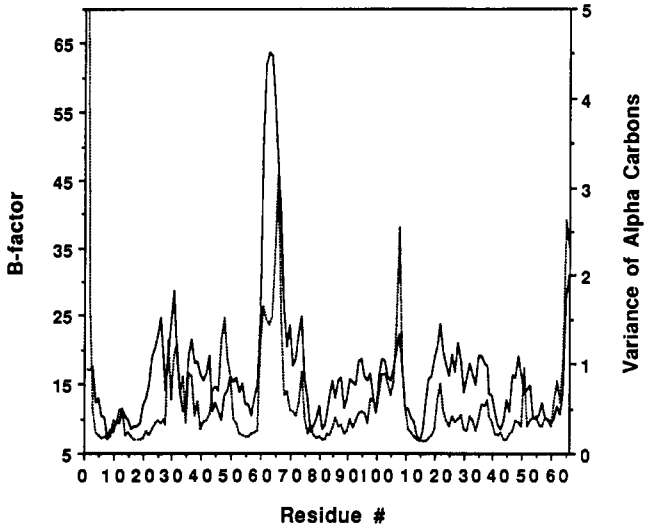

FIGURE 6: *B* factors (solid line) of the C_α atoms of the X-ray structure (Pai et al., 1990) compared to the variance of the average (0–200-ps) simulation structure (dotted line).

considerably over the simulation: τ(9–12) ranges between −40° and −95° (−56.3° average), τ(10–13) between −55° and −110° (−86.7° average), τ(11–14) between 60° and −10° (33.4° average), and τ(12–15) from 130° to 80° (102.8° average). Despite the substantial relative motion implied by these torsion angle changes, the rms comparison of the average structure (174–200 ps) to the X-ray crystal structure of residues 9–15 is 0.39 Å. The variance over the simulation (0–200 ps) shows a small peak at C_α12 (Figure 5); This observation is consistent with the variable P_γ–C_α12 distance.

Several torsion angles define the orientation of the GTP "backbone": (a) the glycosidic bond torsion χ (O4′–C1′–N9–C4) stabilizes at about −153°. This value is consistent with the general anti position of purines (Saenger, 1984); (b) the ribose T angle, which is defined in terms of the five torsion angles about the closed ribose ring (Saenger, 1984), stabilizes at approximately 16°; this defines a C3′ endo conformation for the ribose; (c) the three torsions defining the triphosphate conformation, τ(P_γ–O–P_β–O), τ(O–P_β–O–P_α), and τ(P_β–O–P_α–O), stabilize at approximately 94°, −74°, and −164°, respectively.

(*iv*) *Intramolecular Interactions.* Hydrogen-bonding changes that occur transiently in the simulation are (1) *losses*, the backbone oxygen of G13 with the side chain of K117, the side chain of R149 with the backbone of Q22, the side chain of Q43 with the side chain of T50, the side chain of D69 with the side chain of Q99, and the backbone of G75 with the side chain of K104, and (2) *gains*, the side chain of E3 with the side chain of R41, the side chain of Q43 ($Q_{\epsilon 1}$) with the backbone (HN) of C51, the side chains of R68, Y71, and Y96, the side chains of D69 and R73, and the side chains of D92. As mentioned previously, the β-sheet H-bond at the beginning of the antiparallel β-sheet (between D38 and D57) is lost. The position of the side chain of D57, however, which is bonded to the Mg^{2+} ion through an intervening water in the X-ray crystal structure, maintains this interaction over the simulation. Lys117 maintains a long-range stabilizing interaction with the ribose–guanine complex in both the X-ray and average simulation structures. Likewise, F28, which, in the crystal structure, shows a perpendicular hydrophobic interaction with the guanine opposite Lys117, also does so in the simulation structure. Figure 6 compares the crystal structure *B* factors (Pai et al., 1990) with an estimate of the variance of the average simulation structure (average over 0–200-ps interval) for the α-carbons. Regions of considerable motion in the simulation occur in the 29–32 effector loop, in residues 47–48, in residues 60–68, and near residues 107–108. These observations are largely in agreement with the *B* factors from the 1.35-Å crystal structure. The enhanced motion in the simulation structure near residues 47–48 and 107–108 may be due to the loss of important intermolecular contacts upon solvation at or near the residues. The motion around Gly12 appears to be similar in the simulation and crystal structures. One possible reason for anticipating a difference at C_α12 was that the ligand bound in the crystal structure is the GTP analog GppNp whereas our calculations define the ligand as GTP. The NH of Gly13 interacts with the GppNp NH in the analog and with the ether O in our simulation of the bound GTP. The difference between the ether group and the NH analog is apparently responsible for a 10-fold reduction in the affinity of the analog for the protein (Schlichting et al., 1990), and since Gly13 is adjacent to Gly12, we might have expected to see a dynamical difference at Gly12. Such is not seen. The region of residues 60–68, however, shows the greatest motion both in the *B* factor of the crystal structure and in the variance of the average (0–200-ps) simulation structure (Figure 6).

(*v*) *Structure and Motion of the Protein and Water near the γ-Phosphate.* An analysis of the 1.35-Å crystal structure (Pai et al., 1990) showed considerable motion in residues 60–65. In addition, electron density considerations suggested that the side-chain oxygen of Q61, initially 8.37 Å away from the γ-phosphate, could assume an alternate conformation, approximately 6.0 Å away from the γ-phosphate. In this alternate conformation the O_ϵ of Q61 could possibly activate a water molecule in line for a "head-on" attack on the γ-phosphate. In this alternate conformation, the critical water molecule could be stabilized by the backbone oxygen of T35, and the amino group of Q61 could be stabilized by the side chain of E63. Graphical representations of the X-ray and alternate structure in the region of the γ-phosphate are shown in parts a and b of Figure 7.

An analysis of the γ-phosphate region over the simulation proves very interesting. The tendency of water to localize near the γ-phosphate was examined by performing an analysis of the water mobility near the γ-phosphate. Two solid cones (Figure 8) were defined on the basis of the O_β–P_γ bond, the smaller inner cone using an angle of 45° from the cone axis and a distance from P_γ of 3.5 Å and the second outer cone with an angle of 75° and a distance from P_γ of 6.0 Å. The strategy was to count the elapsed time of water molecule took after entering the smaller solid cone to leave the large cone. Although the water best aligned to effect hydrolysis (water 175 in the PDB file) in the crystal structure had left the γ-phosphate by the end of the equilibration stage, exchange had occurred with another "X-ray" water that then remained well-positioned for hydrolysis for 186 ps—almost the entire simulation. A second water molecule, not of X-ray origin but which originated instead from the box of equilibration water, moved into the cone region of 100 ps and remained for the remainder of the simulation. It is perhaps useful to note that the *B* factor for the water deduced to be critical for hydrolysis in the crystal structure (water 175) is 27.5, substantially higher (more motion) than those, for instance, of the waters bound to the Mg^{2+} ion—11.7 and 8.2, respectively. The cone analysis result suggests that as the simulation proceeds, a water molecule is almost always in a well-aligned position for attack on the γ-phosphate. This observation is completely consistent with the conclusions derived from a study of the crystallographic study (Pai et al., 1990).

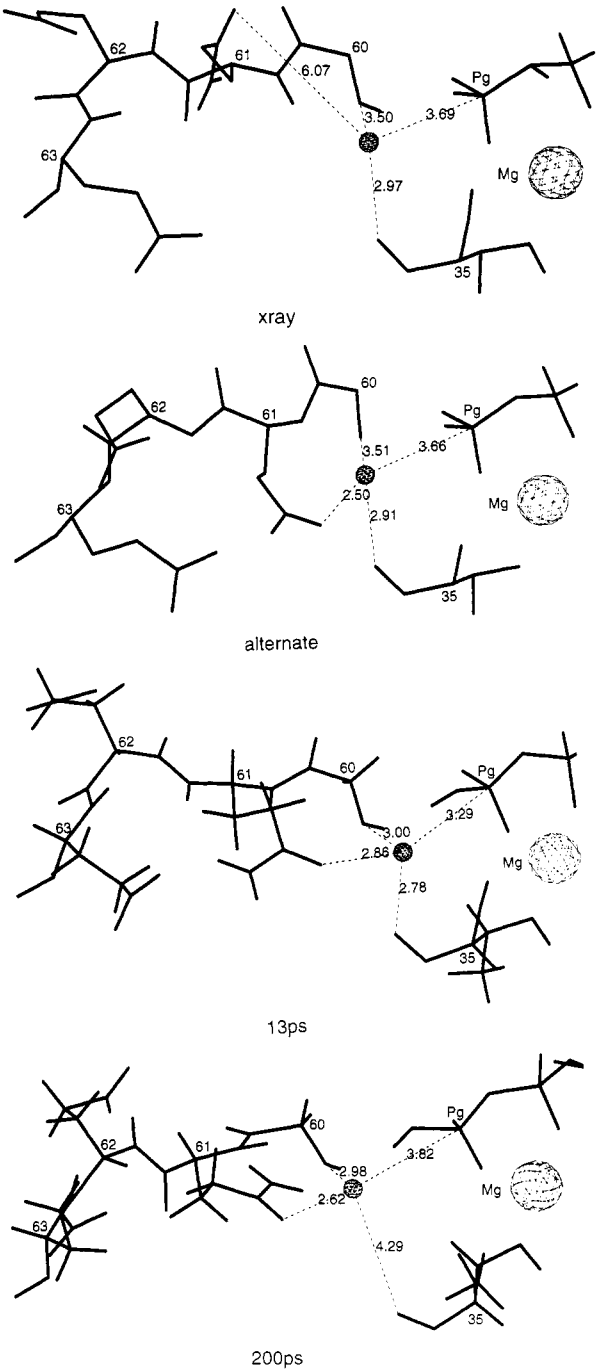

FIGURE 7: The γ-phosphate region (from top to bottom): (a) X-ray crystal structure (Pai et al., 1990); (b) alternate X-ray crystal structure (Pai et al., 1990); (c) simulation structure (13 ps); (d) simulation structure (200 ps). Distances from the water molecule well positioned from hydrolysis to key atoms are given in angstroms.

Is the positioned water molecule in the γ-phosphate region stabilized (or activated) by protein contacts as the alternate conformation of the 60–65 loop suggests? As shown in parts c and d of Figure 7, the side chain of Q61 did, as the simulation proceeded, move closer to the γ-phosphate. A conformation not unlike that of the alternate X-ray structure is adopted by the 60–65 loop at certain times during the simulation. A positioned water (at 13 ps) interacts transiently (Figure 7c) with both the side-chain oxygen of Q61 and with the backbone atoms of T35 in a manner remarkably similar to that proposed by Pai et al. (1990). The $-NH_2$ fragment of the Q61 side chain is stabilized by the side chain of D63. Likewise, another positioned water (200 ps) interacts with the γ-phosphate and O_ϵ of Q61. In this case, the $-NH_2$ side chain of Q61 is stabilized by the side chain of Y64 (not shown). Although it was not certain from crystallographic considerations whether the Q61 side-chain contact with the water molecule was through the O_ϵ or N_ϵ fragments, our unconstrained simulation shows the O_ϵ contact exclusively.

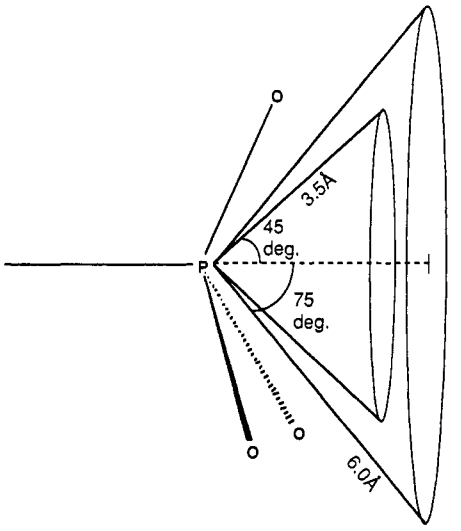

FIGURE 8: Cone definitions used in the analysis of water in the region of the γ-phosphate. The "counting" clock starts when a water molecule enters the inner cone and stops when it leaves the outer cone.

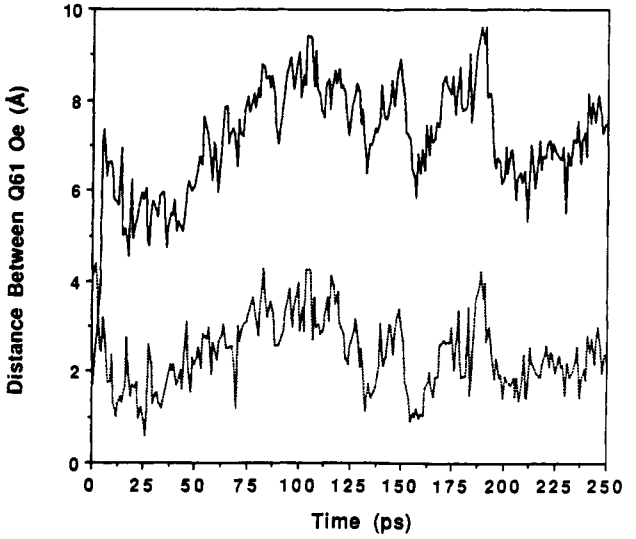

FIGURE 9: Distance between Q61 O_ϵ in the crystal conformations and Q61 O_ϵ in the simulation structure over the simulation (0–249 ps). Structures were overlaid using the backbone atoms of residues 10–59 and 69–156. The main crystal conformation vs simulation is shown with a solid line; the alternate crystal conformation vs simulation is shown with a dotted line.

Overall, we find that the simulation structure has evolved without artificial constrains from the crystallographic structure in which the side chain of Q61 is substantially displaced from the γ-phosphate to a structure in which the side-chain oxygen is reasonably placed to activate a nucleophilic water. That this is the case is emphasized in Figure 9; the simulation structure overlaid onto the "alternate" X-ray structure gives a much better fit for the time dependence of the Q61 O_ϵ position than does the analogous fit made from the overlay of the simulation structure with the X-ray structure.

Conclusion

The simulation presented here emphasizes the dynamic nature of the catalytic region of p21–GTP in both the solution

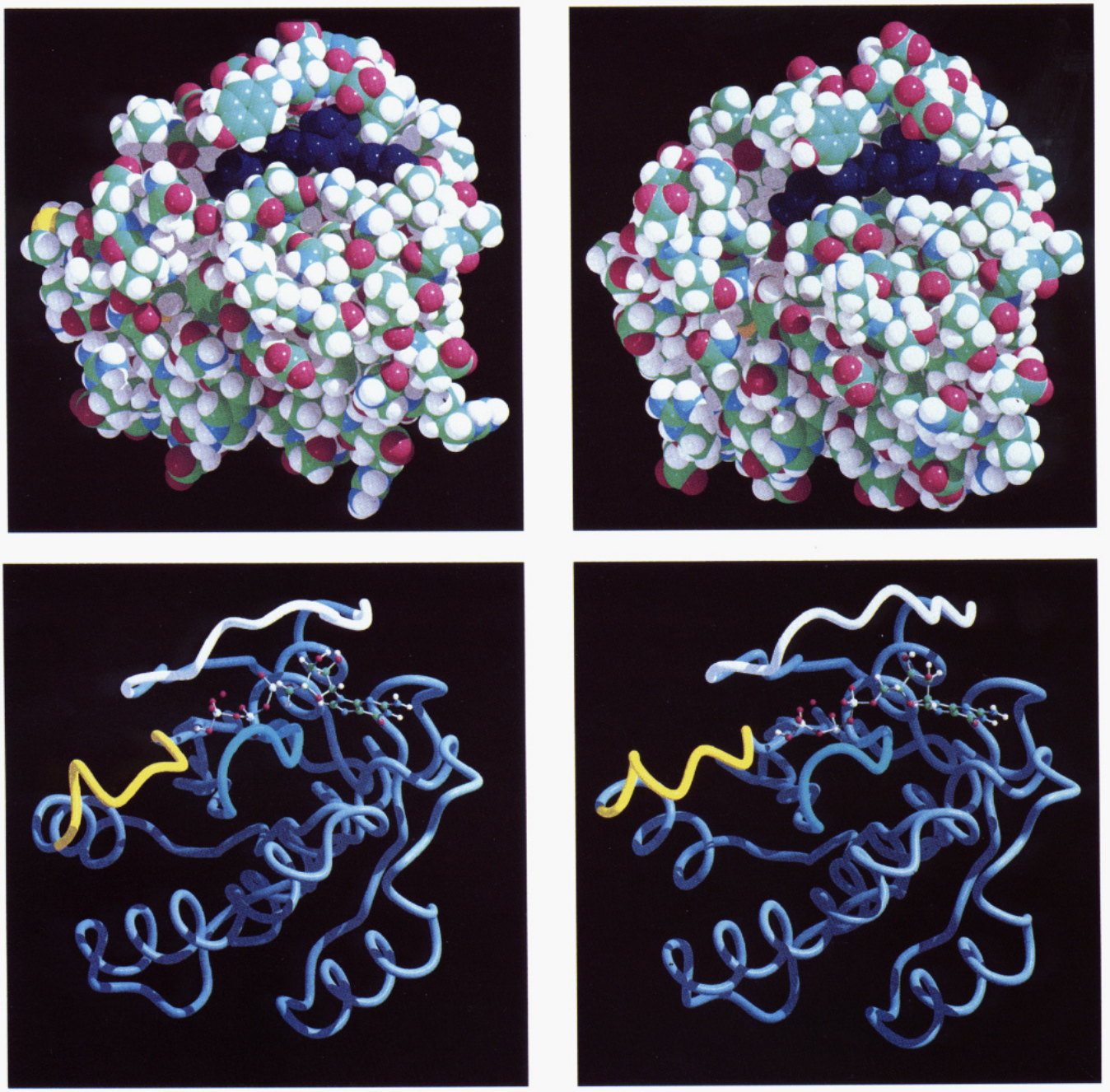

FIGURE 10: Space filling models of (a, top left) the X-ray crystal structure and (b, top right) the average (174–200-ps) solution structure. GTP is shown in dark blue; the γ-phosphate is toward the left and the guanosine toward the right in the figures. "Worm" figures of the backbone trace of (c, bottom left) the X-ray crystal structure and (d, bottom right) the average (174–200-ps) solution simulation structure. Color code: cyan, 10–15 loop (L1); white, 26–36 loop (L2); yellow, 59–65 loop (L4).

and crystalline environments. Since the intrinsic hydrolysis of the GTP in the crystalline system occurs at approximately the same rate as the solution system in the absence of GAP (Schlichting et al., 1989), it is probably reasonable to believe that the γ-phosphate has approximately the same environment in the crystal and solution. We find that the 60–65 loop moves toward the phosphate region in the solution simulation; thus, we conclude that this region may well play a direct role in the solution hydrolysis. We see evidence in the simulation that the side chain of Q61 samples the space around the phosphate and thus could be fulfilling the role envisioned by Pai et al. (1990). Likewise, we find that the T35 O_γ remains mostly near the γ-phosphate in the simulation, and consequently, on the basis of this proximity we would conclude that this side chain could play an important role as a stabilizing group for the transition state involving the nucleophile. That the mutation T35S in c-*ras*^{H} (Willumsen et al., 1989) leads to about a 40% reduction in the GAP-induced hydrolysis rate argues for the involvement of the side chain of T35 in the GTP hydrolysis. That this same mutation in v-*ras*^{H} leads to a total loss of transforming activity (Willumsen et al., 1989) suggests that the side chain of T35 may also be important for sending the growth signal downstream. The side chain of T35 has been shown to dissociate from the Mg^{2+} in some systems (Milburn et al., 1989; Schlichting et al., 1990). It is likewise possible that D57, which also remains in the region of the γ-phosphate, could accept a hydrogen from a water (perhaps one bound to the Mg^{2+} ion) to generate a nucleophilic hydroxide ion active in the hydrolysis. Such a mechanism is thought to occur in staphylococcal nuclease (Weber et al., 1990), in which case a glutamate side chain accepts a proton from a water molecule bound to calcium, and the resultant hydroxide ion attacks a

phosphate that is bound to the calcium.

A graphical summary of the simulation is provided in Figure 10. The space-filling figures (parts a and b of Figure 10) compare the GTP pocket of the X-ray crystal and solution simulation (174–200-ps average) structures; parts c and d of Figure 10 give the same perspective using a "worm" backbone representation. The space-filling models clearly show the solvent accessibility in the GTP region. Only small differences between either of the space filling or either of the worm ray-traced structures (X-ray vs solution) are seen; globally the X-ray crystal and average solution structures are similar. It will be of obvious interest to compare our predicted solution structure with the structure derived from NMR experiments when such is forthcoming.

The methods used in this work are subject to a number of caveats. Among these we mention the following: (a) the force field model employed is very simple in that it does not explicitly account for cross terms, although inclusion of these may not be so important for solution studies unless spectra (IR) are being simulated; (b) the charge distribution is defined by a set of static point charges; i.e., possible charge exchange or polarization is not accounted for; (c) the rigid water model (TIP3P), while standard in application, is exceedingly simple; (d) the counterion description (with the exception of the Mg^{2+} ion) is reasonable, but fictitious, and does not include small ions of opposite charge, such as chlorides, which are undoubtedly present; and (e) the cutoff used for the nonbonded interactions, even with the large (22-Å) values used herein, must ultimately, in a very long simulation, lead to spurious behavior. Nevertheless, given that the molecule studied here has no stabilizing disulfide bonds and that the ionic interactions are many, the lengthy simulation is remarkably stable. This apparent stability, coupled with the evolution of the X-ray to the alternate structure (for residues 60–65), gives encouragement for dealing with difficult systems.

Added in Proof

We have recently performed a similar simulation using mass = 1 amu for hydrogens and an update of the nonbonded forces every 10 steps. Results are similar to those reported here except that the side chain of Lys16 remains in contact with the γ-phosphate and Ala18 remains in contact with the α-phosphate group.

Acknowledgments

L.G.P. thanks the NIEHS for a 1-year EXPERT appointment. T.A.D. benefited greatly from conversations with C. Sander and P. Stouten at the EMBO, Heidelberg. We thank the National Cancer Institute for use of their Cray Y-MP supercomputer and the North Carolina Supercomputing Center for access to their Cray Y-MP during its installation/testing phase. We also thank H. C. Smith at the NIEHS for assistance with data analysis and presentation and T. Palmer of Cray Research, Inc., for his assistance with the ray-traced figures.

References

Adari, H., Lowy, D. R. Willumsen, B. M., Der, C. J., & McCormick, F. 91988) *Science 240*, 518–521.

Baldwin, E. T., Weber, I. T., St. Charles, R., Xuan, J.-C., Appela, E., Yamda, M., Matsushima, K., Edwards, B. F. P., Clore, G. M., Groneborn, A. M., & Wlodawer, A. (1991) *Proc. Natl. Acad. Sci. U.S.A. 88*, 502–506.

Bax, A. (1989) *Annu. Rev. Biochem. 58*, 223–256.

Berendsen, H. J. C., Van Gunsteren, W. F., Zwinderman, H. R. J., & Geurtsen, R. G. (1986) *Ann. N.Y. Acad. Sci. 482*, 269–286.

Bollag, G., & McCormick, F. (1991) *Nature 351*, 576–579.

Bourne, H. R., Sanders, D. A., & McCormick, F. (1991) *Nature 349*, 117–127.

Chirlian, L. E., & Francl, M. M. (1987a) *J. Comput. Chem. 8*, 894.

Chirlian, L. E., & Francl, M. M. (1987b) *QCPE Bull. 7*, 39.

Darden, T., Johnson, P., & Smith, H. (1991) *J. Mol. Graphics 9*, 18–23.

Downward, J., Riehl, R., Wu, L., & Weinberg, R. A. (1990) *Proc. Natl. Acad. Sci. U.S.A. 87*, 5998–6002.

Frisch, M. J., Head-Gordon, M., Schlegel, H. B., Raghavachari, K., Binkley, J. S., Gonzalez, C., Defrees, D. J., Fox, D. J., Whiteside, R. A., Seeger, R., Melius, C. F., Baker, J., Kahn, L. R., Stewart, J. J. P., Fluder, D. M., Topiol, S., & Pople, J. A. (1988) *Gaussian 88*, Gaussian, Inc., Pittsburgh, PA.

Gibbs, J. B., Schaber, M. D., Allard, W. J., Sigal, I. S., & Scolnick, E. M. (1988) *Proc. Natl. Acad. Sci. U.S.A. 85*, 5026–5030.

Jorgensen, W. L., Chandrasekhar, J., Madura, J. D., Impey, R. W., & Klein, M. L. (1983) *J. Chem. Phys. 79*, 926–935.

Kabsch, W. (1976) *Acta Crystallogr. A32*, 922–923.

Kabsch, W. (1978) *Acta Crystallogr. A34*, 827–828.

Kabsch, W., & Sander, C. (1983) *Biopolymers 22*, 2577–2637.

Levitt, M., & Sharon, R. (1988) *Proc. Natl. Acad. Sci. U.S.A. 85*, 7557–7561.

Loncharich, R. J., & Brooks, B. R. (1989) *Proteins 6*, 32–45.

McCammon, J. A., & Harvey, S. (1987) in *Dynamics of Proteins and Nucleic Acids*, pp 176–180, Cambridge University Press, Cambridge.

McCormick, F. (1989) in *Oncogenes and the Molecular Origin of Cancer* (Weinberg, R. A., Ed.) pp 125–145, Cold Spring Harbor Press, Cold Spring Harbor, NY.

Milburn, M. V., Tong, L., DeVos, A. M., Brunger, A., Yamaizumi, Z., Nishimura, S., & Kim, S.-H. (1990) *Science 247*, 939–945.

Pai, E., Kabsch, W., Krengel, U., Holmes, K., John, J., & Wittinghofer, A. (1989) *Nature 341*, 209–214.

Pai, E. F., Krengel, U., Petsko, G. A., Goody, R. S., Kabsch, W., & Wittinghofer, A. (1990) *EMBO J. 9*, 2351–2359.

Ryckaert, J. P., Ciccotti, G., & Berendsen, H. C. (1977) *J. Comput. Phys. 23*, 327–341.

Saenger, W. (1984) in *Principles of Nucleic Acid Structure*, Springer-Verlag, New York.

Schlichting, I., Rapp, G., John, J., Wittinghofer, A., Pai, E. F., & Goody, R. S. (1989) *Proc. Natl. Acad. Sci. U.S.A. 86*, 7687–7690.

Schlichting, I., Almo, S. C., Rapp, G., Wilson, K., Petratos, K., Lentfer, A., Wittinghofer, A., Kabsch, W., Pai, E. F., Petsko, G. A., & Goody, R. S. (1990) *Nature 345*, 309–315.

Smith, P. E., & Pettitt, B. M. (1991) *J. Chem. Phys. 95*, 8430–8441.

Swope, W. C., & Andersen, H. C. (1990) *Phys. Rev. B 41*, 7042–7054.

Valencia, A., Chardin, P., Wittinghofer, A., & Sander, C. (1991) *Biochemistry 30*, 4637–4648.

Vogel, U. S., Dixon, R. A. F., Schaber, M. D., Diehl, R. E., Marshall, M. S., Scolnick, E. M., Sigal, I. S., & Gibbs, J. B. (1988) *Nature 335*, 90–93.

Weber, D. J., Serpersu, E. H., Shortle, D., & Mildvan, A. S. (1990) *Biochemistry 29*, 8632–8642.

Weiner, S. J., Kollman, P. A., Case, D. A., Singh, U. C., Chio, C., Alagona, C., Profeta, S., Jr., & Weiner, P. (1984) *J.*

Am. Chem. Soc. 106, 765–784.
Weiner, S. J., Kollman, P. A., Nguyen, D. T., & Case, D. A. (1986) J. Comput. Chem. 7, 230–252.
Willumsen, B. M., Adari, H., Zhang, K., Papageorge, A. G., Stone, J. C., McCormick, F., & Lowy, D. R. (1989) in The Guanine Nucleotide Binding Proteins, NATO ASI Series A, Vol. 165, pp 165–177, Plenum, New York.
Yamasaki, K., Kawai, G., Ito, Y., Muto, Y., Fujita, J., Miyazawa, T., Nishimura, S., & Yokoyama (1989) Biochem. Biophys. Res. Commun. 162, 1054–1062.

Crystal Structure of an Electron-Transfer Complex between Methylamine Dehydrogenase and Amicyanin[†,‡]

Longyin Chen,[§] Rosemary Durley,[§] Barbara J. Poliks,[§] Kensaku Hamada,[§] Zhiwei Chen,[§] F. Scott Mathews,*[,§] Victor L. Davidson,[∥] Yoshinori Satow,[⊥] Eric Huizinga,[#] Fred M. D. Vellieux,[#] and Wim G. J. Hol[#]

Department of Cell Biology and Physiology, Washington University School of Medicine, St. Louis, Missouri 63110, Department of Biochemistry, University of Mississippi Medical Center, Jackson, Mississippi 39216, Photon Factory, National Laboratory for High-Energy Physics (KEK), Tsukuba, Ibaraki 305, Japan, and Bioson Research Institute, University of Groningen, 9747 AG Groningen, The Netherlands

Received February 11, 1992; Revised Manuscript Received March 24, 1992

ABSTRACT: The crystal structure of the complex between the quinoprotein methylamine dehydrogenase (MADH) and the type I blue copper protein amicyanin, both from *Paracoccus denitrificans*, has been determined at 2.5-Å resolution using molecular replacement. The search model was MADH from *Thiobacillus versutus*. The amicyanin could be located in an averaged electron density difference map and the model improved by refinement and model building procedures. Nine β-strands are observed within the amicyanin molecule. The copper atom is located between three antiparallel strands and is about 2.5 Å below the protein surface. The major intermolecular interactions occur between amicyanin and the light subunit of MADH where the interface is largely hydrophobic. The copper atom of amicyanin and the redox cofactor of MADH are about 9.4 Å apart. One of the copper ligands, His 95, lies between the two redox centers and may facilitate electron transfer between them.

Many methylotrophic bacteria, when grown on methylamine as the sole source of carbon and energy, synthesize a soluble periplasmic methylamine dehydrogenase (MADH)[1] (de Beer et al., 1980). MADH catalyzes the oxidative deamination of primary amines and donates electrons to one or more *c*-type cytochromes, through a mediating blue copper protein called amicyanin (Husain & Davidson, 1985, 1986).

MADH is a heterotetramer consisting of two identical heavy (H) and two identical light (L) subunits. The enzyme from *Paracoccus denitrificans* (PD-MADH) has subunit molecular masses of 46.7 and 15.5 kDa, respectively (Husain & Davidson, 1987). The redox cofactor of MADH has been shown to be tryptophan tryptophylquinone (TTQ, Figure 1), which is composed of a pair of posttranslationally modified tryptophan residues of the L subunit which are cross-linked and contain an *o*-quinone group on one of them (McIntire et al., 1991; Chen et al., 1991).

To date no complete amino acid sequence of MADH from any source has been reported. The amino acid sequence (Ishii et al., 1983) and DNA sequence (Chistoserdov et al., 1990) of the L subunit of the enzyme from *Methylobacterium extorquens* AM1 (formerly called *Pseudomonas* AM1) have been determined. The crystal structure of MADH from *Thiobacillus versutus* (TV-MADH) has been reported recently and an amino acid sequence deduced from the electron density at 2.25-Å resolution of both the H and L subunits (Vellieux et al., 1989, 1990). The latter structure was used as the search model for molecular replacement to solve the crystal structure of MADH from *P. denitrificans* (Chen et al., 1992).

The amino acid sequence of the amicyanin of *P. denitrificans* has been determined (van Spanning et al., 1990), and the protein was shown to have a molecular mass of 12.5 kDa. Most of the physical, redox, and spectroscopic properties of amicyanin are very similar to those of other small blue copper proteins such as azurin and plastocyanin. Available amino acid sequence data indicate that amicyanins are a separate and unique class of copper proteins bearing closest similarity with plastocyanin (van Beeumen et al., 1991). Resonance Raman spectroscopic studies (Sharma et al., 1988) and two-dimensional NMR studies (Lommen et al., 1988) support this claim.

The specificity of interaction between amicyanin and MADH has been best demonstrated by studies of the proteins isolated from *P. denitrificans*. Each of these proteins is induced in this bacterium only during growth on methylamine

[†] This work is supported by NSF Grant DMB-8816618 and USPHS Grant GM41574 and by the Netherlands Foundation for Chemical Research (SON) with financial aid from the Netherlands Organization for Scientific Research (NWO).

[‡] Crystallographic coordinates have been deposited in the Brookhaven Protein Data Bank under the file name IMDA.

* To whom correspondence should be addressed.
[§] Washington University School of Medicine.
[∥] University of Mississippi Medical Center.
[⊥] National Laboratory for High-Energy Physics (KEK).
[#] University of Groningen.

[1] Abbreviations: MADH, methylamine dehydrogenase; PD-MADH, *Paracoccus denitrificans* methylamine dehydrogenase; rms, root mean square; TV-MADH, *Thiobacillus versutus* methylamine dehydrogenase; TTQ, tryptophan tryptophylquinone.

0006-2960/92/0431-4959$03.00/0